Synthesis and Characterization of Functionalized Se-MCM-41 a New Drug Carrier Mesopore Composite

M. M. RAHMAN[1], M.A.B.M. AZNAN[2*], A. M.YUSOF[2],

H.ANSARYR[1], M. J. SIDDIQI[1] and S. YUSAN[4]

[1]Faculty of Pharmacy, International Islamic University Malaysia, 25200 Kuantan, Malaysia.
[2]Faculty of Medicine, Islamic University Malaysia, 25200 Kuantan, Malaysia.
[3]Faculty of Science, UniversitiTeknologi Malaysia, 81310 Johor Bahru, Malaysia.
[4]Institute of Nuclear Science, Ege University, 35100 Bornova, Izmir, Turkey.
[*]Corresponding Author E-mail: aznan@iium.edu.my

ABSTRACT

Various nanocomposite materials play a number of important roles in modern science and technology including pharmaceutical science. Among these materials, mesoporous materials cover a large number of applications in drug delivery system. The quantitative incorporation and high dispersion of selenium nanoparticles into MCM-41 have been made possible by the coordination between Se(IV) ion and aminopropyltriethoxysilane (APTES)-anchored MCM-41. The samples were characterized by X-ray powder diffraction, Fourier-transformed infrared spectroscopy (FTIR), scanning electron microscopy (SEM), nitrogen adsorption–desorption via multi-point Brunauer, Emmett and Teller (BET) analysis, Raman spectroscopy and UV-Vis diffusion reflection spectroscopy (UV-vis/DRS). The increase in cell parameter and the decrease in surface area observed by N_2 adsorption-desorption technique were taken as evidence of selenium introduction inside the MCM-41 framework. The behaviour of drug release in these nanocomposites is probably due to hydrogen bonding interactions between drug and the hydroxyl group on the composite framework.

Keywords: Mesoporous materials, MCM-41, Se-MCM-41.

INTRODUCTION

Mesostructured silica particles have many attractive features such as high pore volume, large surface area and narrow pore size and ease of functionalization[1, 2]. One of the most well known mesoporous molecular sieves, M41S, has attracted much attention since it was first developed by researchers at Mobil Corporation in the year of 1990. Due to its excellent properties such as high surface area, well defined regular pore shape, narrow pore size distribution, large pore volume,

tunable pore size and thermal stability, MCM-41 has been utilized for chemical and environmental application as adsorbents, catalyst support systems, ion-exchanged materials and nanofilters. MCM-41 is a member of this group and has unidimensional pores with a hexagonal structure and high surface area[3]. These properties together with the thermal and mechanical stabilities make it an ideal host for the incorporation of active molecules and some work has already been devoted on this field[4-6]. Many studies have been carried out on the incorporation of various transition metals (Al, Co, Zn, Mn, Ce, Ti, Fe, V, Ga etc.) into the framework of MCM-41 in order to improve the catalytic properties of MCM-41[7-14]. However inorganic materials (clay, zeolite and MCM-41) have important advantages such as high chemical and mechanical stability and low toxicity and porous structure that can be tailored to control the diffusion rate of an adsorbed or encapsulated drug; but these materials have some problems when using them in aqueous solutions and are less studied as carriers of drugs compared to organic materials such as polymers[15-16]. Although, controlled drug delivery technologies using polymers as carriers, including natural or synthetic polymers, represent one of the most rapidly advancing areas of science[17].

Nanometer-sized semiconductor particles have great importance because of their electrical and optical properties. Among the semiconductor particles, selenium (Se) is well known for its unique mechanical, optical, electrical, biological and chemical properties[18]. In addition, selenium is one of the essential trace elements for human health because it exerts anti-oxidative and pro-oxidative effects[19]. Selenium can improve the activity of the seleno-enzyme, glutathione peroxidase and prevent free radicals from damaging cells and tissues *in vivo*[20]. Selenium occurs in four known modifications: amorphous, hexagonal, monoclinic-α and monoclinic-β . The Se atoms in the solid state are arranged in a ring or chain formation. Rings of eight atoms (Se_8) are characteristic for monoclinic selenium, and rings with a larger number of atoms (Se_{6-1000}) for amorphous selenium; hexagonal selenium is formed by long chains. Amorphous and monoclinic selenium are typical insulators, while hexagonal selenium is a typical semiconductor[21].

Herein, in this study, we report the synthesis of a new selenium-functionalized MCM-41 mesoporous hybrid material in which nano-selenium was covalently bonded to the framework of MCM-41 by 3-(Triethoxysilyl)-propylamine (APTES). Full characterization and detailed studies of all these synthesized materials were investigated. Uniform hexagonal selenium nanoparticles were synthesized via chemical reduction. The materials were characterized by XRD, FTIR, BET, UV-Vis/DRS, SEM and Raman spectroscopy. The morphological features of the mesostructure and the selenium ions incorporated in the Se-MCM-41 were subsequently investigated.

EXPERIMENTAL

Materials

The synthesis of MCM-41 was carried out by using Ludox HS-40 (Sigma 40 % w/t) with cetyltrimethylammonium bromide (CTAB,
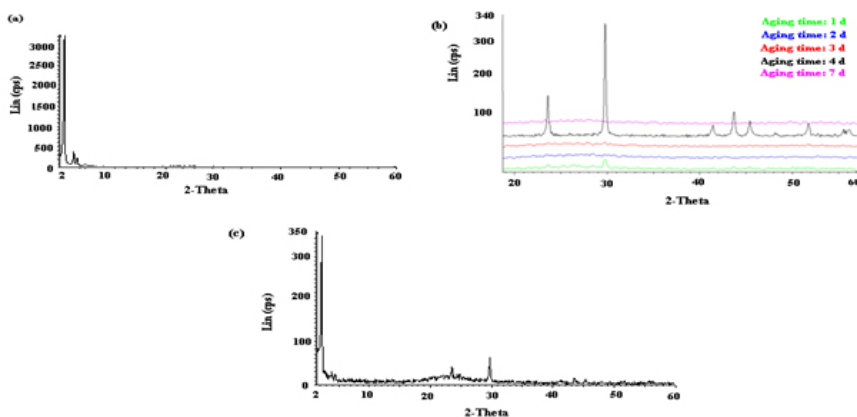

Fig. 1: XRD patterns of MCM-41 (a), Se nanoparticles (b), Se-MCM-41 (c).

Aldrich) and hexadecyltrimethylammonium bromide (HDTMA, Acros), as the silica source and precursor agents, respectively. Selenious acid (H_2SeO_3), sodium hydroxide, ammonium hydroxide, ascorbic acid, acetic acid and chloroform were of analytical grade and obtained from Merck (Germany). (3-Aminopropylaminopropyl)-triethoxysilane (APTES) was purchased from Aldrich (Germany). All materials were of Annular Grade and were used as purchased without further purification. All aqueous solutions were prepared with de-ionized water (DW) which is purified with Millipore Milli-Q Plus water purification system.

Synthesis procedures
Preparation of MCM-41 mesoporous material
MCM-41 was prepared using the hydrothermal method. Accurately weighed 27.8715 g of Ludox HS-40 (silica source) was dissolved in NaOH (4.49 %) in a polypropylene bottle followed by stirring for 30 min at 80ºC. The template solution was prepared by dissolving 11.1308 g CTAB in distilled water and appropriate NH_4OH (28 %) added later and stirred for 1 h at 80ºC. At the end of the reaction time, both Ludox HS-40 and the CTAB solutions were cooled to 40ºC and later mixed, followed by aging at 97ºC for 24 h with its pH adjusted to 10.2 with acetic acid. This procedure was repeated three times. The precipitated MCM-41 products were filtered and washed with DW in order to remove excess surfactants that did not participate in the formation of the mesostructures. Finally, the remaining CTAB surfactant was removed by calcination at 550ºC for 24 h in a furnace.

Preparation of selenium nanoparticles
The selenium nanoparticles were synthesized from 0.25 M H_2SeO_3 and 0.25 M ascorbic acid. The solution was treated by ultra-sonication for 3 h. Different aging times of 1, 2, 3, 4 and 7 days were chosen to determine the optimized conditions for excellent Se nanoparticles crystal growth. The final product was filtered and washed with DW and left overnight for drying.

Preparation of Se- MCM-41 mesoporous material using APTES
Typically 1 g MCM-41 and 0.1 g Se nanoparticles were ground and a 0.5 M (100 ml) APTES (in chloroform) later added to the mixture in the preparation of Se-MCM-41. The mixture was later ultrasonicated for 4 h followed by stirring for 24 h, then filtered and washed three times with chloroform.

Characterization
XRD
The X-Ray diffraction analysis of MCM-41, Se nanoparticles and Se-MCM-41 composite were performed in the range of $2\theta = 5°$ to $50°$ using a Siemens 5000 diffractometer with a vertical goniometer and CuKα radiation (λ= 1.542 Å) at 35 kV and 35 mA (scanning speed: 4°/min).

FTIR
Infrared spectra were recorded with a Perkin-Elmer Spectrum One in KBr matrix (0.005 g sample with 0.1g KBr) in the range of 4000–400 cm^{-1}.

N₂-Adsorption-desorption
Nitrogen gas adsorption-desorption isotherms were measured at the liquid N_2 temperature of 77K using a Quantachrome Autosorb-1 instrument (QUANTACHROME, version 1.51). Prior to the sorption experiment, the materials were vacuum-
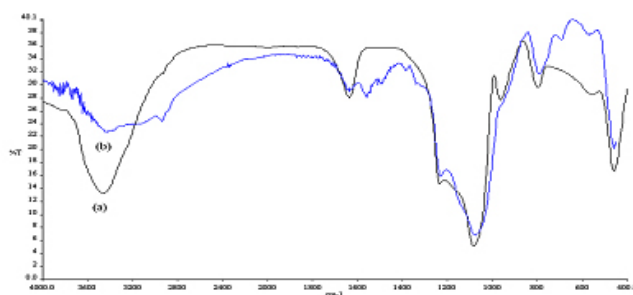

Fig. 2. FT-IR spectra of MCM-41 (a) and Se-MCM-41 (b)

Fig.2: FT-IR spectra of MCM-41 (a) and Se - MCM-41 (b)

dried at 120°C for 6 h. Surface area, pore size and pore volumes of the samples were obtained from these isotherms using the conventional BET and BJH equations. Specific surface area (S_{BET}) was determined by the Brunauer–Emmett– Teller (BET) method using adsorption data points in the relative pressure P/Po range of 0.02–0.80. The surface area of Se-MCM-41 (St) was also determined from t-plots which were constructed using the nitrogen adsorption data on a nonporous-hydroxylated silica standard.

Scanning electron microscope (SEM)

The morphology of the samples was inspected in a Philips equipment model XL 40, operating at 25 kV. The samples were supported on carbon tapes and then metalized with gold under vacuum conditions.

FT-Raman

The FT-Raman spectrum was recorded with Spectrum 2000R NIR FT-Raman system in a Perkin-Elmer Spectrum GX model equipped with aNd-YAG laser (1064 nm). A laser power of about 15 mW was used for excitation in the range of 1500 and 100 cm⁻¹ with 10 scans and spectral resolution of about 4 cm⁻¹.

UV-visible/Diffuse reflectance spectroscopy

UV-Vis Diffuse Reflectance (UV-Vis DR) of the samples was recorded using a Perkin Elmer Lambda 900 UV-VIS-NIR spectrometer in the wavelength range of 200–800 nm.

RESULTS AND DISCUSSIONS

Characterization

Synthesized products were characterized by XRD, FTIR, SEM, FT-Raman and UV-Vis/ DRS. Surface area and pore-size distribution of the synthesized materials were inspected by nitrogen adsorption method. Specific surface areas were calculated following the BET procedure. Pore-size distribution was obtained by using the BJH pore analysis applied to the desorption branch of the nitrogen adsorption/desorption isotherms.

XRD

Powder X-ray diffraction patterns of MCM-41, selenium nanoparticles and Se-MCM-41 samples are shown in Figs. 1 (a), (b) and (c), respectively. XRD analysis was used to characterize the MCM-41, the crystallinity of the Se prepared at various aging times and Se-MCM-41 mesopore composite. The X-ray diffractograms of MCM-41, Se and Se-MCM-41
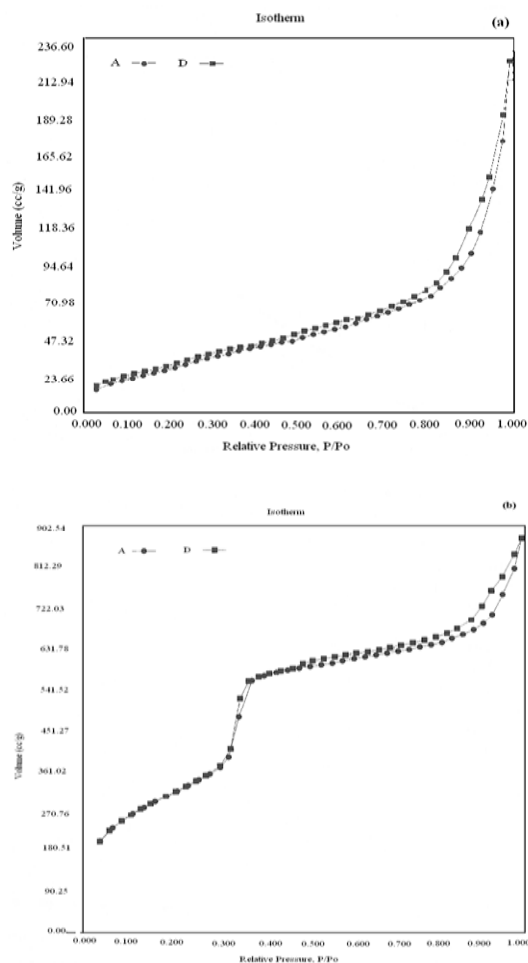

Fig. 3: Nitrogen adsorption (·) and desorption (%) isotherm curves of MCM-41 (a) and Se-MCM-41 (b)

Table 1: Structural data of MCM-41 and Se–MCM-41 samples (S_{BET}, specific surface area; Vt, total pore volume; w, pore width; t, wall thickness)

Samples	S_{BET} (m² g⁻¹)	V_t (cm³ g⁻¹)	w (nm)	t (nm)
MCM-41	203	0.320	6.300	1.324
Se-MCM-41	36.9	0.025	2.713	2.088

indicated a sharp d_{100} reflection line in the 2θ range $2.187°$, $29.80°$ and $2.181°$, respectively.

MCM-41 showed a typical mesoporous structure with three sharp peaks at low 2q values that can be indexed as (1, 0, 0), (1, 1, 0) and (2, 0, 0) reflections characteristics of mesoporous materials with hexagonal arrangement of their cylindrical channels (Fig. 1(a))[22, 23]. As seen from Fig. 1(b), the aging time has a profound effect on the structure of selenium. The diffractogram showed a clear broad peak with some sharp ones, as depicted in Fig. 1 (b) for the aging time of 4 days. Also, the broad halo peaks showed that a large fraction of the Se nanomaterials was in the amorphous state for other aging times. The presence of a hexagonal phase was clearly discernible. The peak positions and their relative intensities are very consistent with the presence of a hexagonal selenium phase with random crystallographic orientations. Similar results were obtained for the selenium particles. From this XRD pattern, all of the peaks could be indexed as hexagonal selenium according to the standard card (JCPDS 06-0362) with the lattice constants a: 0.4366 nm, c: 0.4953 nm[21, 24-26].

Characteristic peaks of the hexagonal system were also found for the Se-MCM-41 sample. No change in the XRD pattern and d-spacing values was observed after functionalization, thus indicating that the functionalization of MCM-41 did not lead to a structural change. The intensity of the three peaks for Se–MCM-41 decrease was compared with those of MCM- 41. It suggests that the long-range order of the sample is not as good as that of MCM-41 and may be due to the incorporation of Se and amino groups into the framework of MCM-41[27- 29].Traditionally, the broadening of peaks in XRD patterns of polycrystalline solids is attributed to particle size effects. The mean crystallite size of a powder sample is estimated from the full-width at half-maximum (FWHM) of the diffraction peak according to the Scherrer equation:

$$d = k\lambda/\beta(\cos 2\theta/2) \qquad ...(1)$$

In this equation, d is the average particle size (nm), λ is the X-ray wavelength (λ=0.154nm), K is the constant (K=0.90), β is the full width at half maximum (FWHM) of the most intense peak, and θ is the corresponding diffraction angle. The Scherrer formula to estimate particle size is widely used, especially in the study of nanoparticulate materials[30-31].The XRD patterns indicated that the samples formed are comparatively of high purity. Therefore, the size of the Se nanoparticles and MCM-41 calculated according to Eq (1) were 41 nm and 215 nm, respectively.
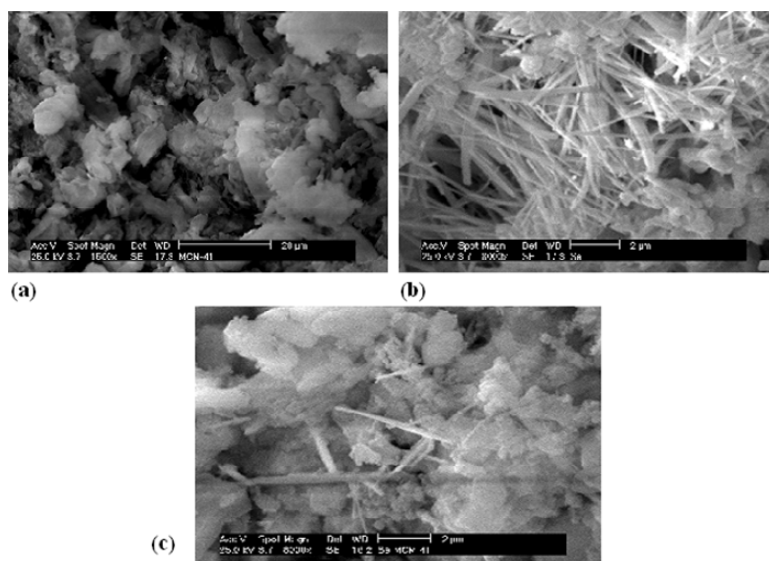

Fig. 4: SEM images of the synthesized materials: MCM-41 (a), Se (b), and Se-MCM-41 (c), respectively.

FTIR

The FT-IR spectra of as-synthesized and amine modified samples are shown in Fig. 2. For MCM-41, the strongest bands relative to those of the silica host structure appear between 1000 and 1250 cm^{-1} and are due to Si-O asymmetric stretching vibrational modes, which is seen in all the figures. The band at ca. 799 cm^{-1} can be attributed to the Si-O symmetric vibrational mode and the Si-O-Si bending vibration is found at ca. 459 cm^{-1}. The presence of water molecules is shown by the presence of a strong band at ca. 1637 cm^{-1} [32]. Fig. 2 also shows a broad band in the range of 3750–3000 cm^{-1} due to OH stretching vibrations from silanol groups and adsorbed water and a band in the range of 1650–1630 cm^{-1} which is due to the OH bending from adsorbed water molecules. Upon silylation, the FTIR spectra of all materials show bands characteristics of the grafted organosilanes, typically in the regions of 3000–2500 and 1650–1300 cm^{-1} [33]. The spectra showed a broad band around 3100–3600 cm^{-1} which is due to adsorbed water molecules. The presence of N-H bending vibration at 695 cm^{-1} and NH$_2$ symmetric bending vibration at 1559 cm^{-1}, absent in neat MCM-41, indicates the successful grafting of organic amine onto the surface. NH$_2$-Si-MCM-41 shows a band at ca. 3444 cm^{-1} which is characteristics of the NH$_2$ groups and a band due to asymmetric vibration of the CH$_2$ groups of the propyl chain of the silylating agent at 2935 cm^{-1} [32,34,35]. The spectra from APTES display bands at 3600-3050 cm^{-1} corresponding to NH and OH groups while the band at 2935 cm^{-1} is due to the stretching vibration of CH$_2$. Bands in the 1500-800 cm^{-1} frequency range characterize stretching vibrations mode of C-N bonds (CN) of the

surface groups and the bands at 1637 cm^{-1} and 1556 cm^{-1} are assigned to the CO amide I and NH amide II groups and the one at 1087 cm^{-1} is assigned to SiO vibrationl.

Compared to the Si-MCM-41, the wave number of the antisymmetric Si-O-Si vibration band of Se-MCM-41 sample decreases to 1075 cm^{-1} (Figs. 2(a) and (b)). Theses shifts must be due to the increase of the mean Si-O distance in the walls caused by the substitution of the small silicon(radius 40 pm) by the larger size Se (radius 50 pm). The observed shifts, which depend on the change in the ionic radii as well, as on the degree of substitution, are comparatively small. Therefore, only a low degree of substitution is suggested[37].

Nitrogen adsorption-desorption isotherms

N$_2$ adsorption-desorption is a common method to characterize mesoporous materials. This method provides information about the specific surface area, average pore diameter and pore volume, etc. BET surface area, S$_{BET}$, pore size, w, pore volume, Vt, and pore wall thickness, t for the synthesized materials are presented in Table 1. The specific surface area (S$_{BET}$) was calculated according to the standard BET method. The cylinder diameter size (w) was calculated by the BJH method and the total pore volume (Vt) was obtained from the nitrogen amount adsorbed in correspondence of P/P$_0$ equal to 0.02. The pore wall thickness (t) was then estimated using the following equation:
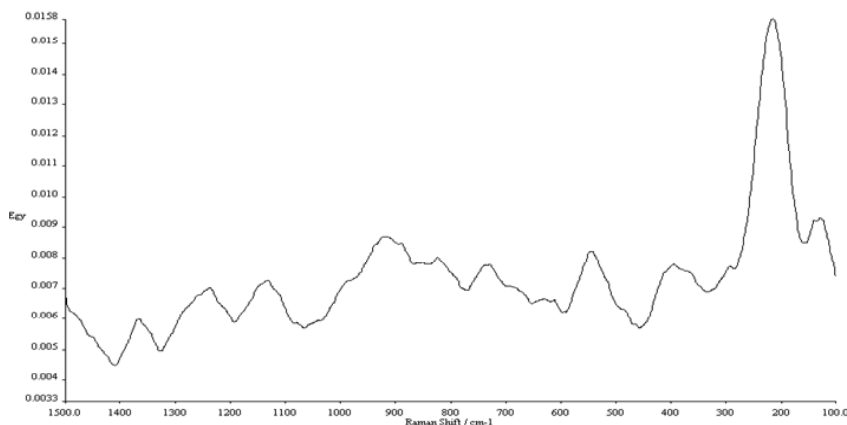
$$t = a_0 - kw \qquad ...(2)$$

Fig. 5: Raman spectra of Se-MCM-41

where k is a constant that of hexagonal cylinder and pore wall mass density was obtained by using geometrical consideration equal to 0.95 w. From the XRD, the average pore diameter, a_0, can be calculated using d_{100} space values which is correlated with the adjacent pores centre-centre distance. The equation is shown below[38-41]

$$a_0 = 2d_{100}/\sqrt{3} \qquad \qquad ...(3)$$

The results show that the surface properties of the modified (Se-MCM-41) are clearly different from the unmodified (MCM-41) since MCM-41 has larger surface area compared to Se-MCM-41. The modification leads to a reduction in surface area, pore volume and pore diameter and the pore wall thickness, estimated on the basis of the Eq. (2), increases. This is probably due to the occupation of the functionalized molecules on the surface and inside the pores of the composite[27, 34].

As shown in Figs. 3 (a) and (b), MCM-41 and Se-MCM-41 exhibited a characteristic type IV BET isotherm consistent with the presence of cylindrical mesoscale pores. It is observed that there are three different well-defined stages in the isotherm. The initial increase in nitrogen uptake at low P/P_0 may be due to monolayer adsorption on the pore walls, a sharp steep increase at intermediate P/P_0 may indicate the occurrence of a capillary condensation in the mesopores and a plateau portion at higher P/P_0 is associated with multilayer adsorption on the external surface of the materials.

A hysteresis of H_3 type at $P/P_0 > 0.9$ was observed for the modified sample. MCM-41 sample exhibits isotherm with well-developed steps in the relative pressure range $\approx$ 0.3, characteristic of a capillary condensation into uniform mesopores[35]. From the two branches of adsorption–desorption isotherms, the presence of a sharp adsorption step in the P/P_0 region from 0.3 to 0.5 and an H_1 type hysteresis loopat the relative pressure $P/P_0 > 0.35$ shows that all materials possess a well-defined array of regular mesopores. From the figure, one can see that all the samples possess good mesoporous structural ordering and a narrow pore size distribution[22].

SEM

The scanning electron microscope (SEM) images illustrated in Figs. 4(a), 4(b), and 4(c) reveal the general morphology of MCM-41, selenium, and Se-MCM-41, respectively. The SEM micrograph of MCM-41 (Fig.4 (a)) demonstrated a variety of particle shapes and sizes.The SEM images of the samples (Fig. 4) confirmed the expected particles morphology. The SEM of selenium (Fig.4 (b)) showed straight rod shapes as expected for the hexagonal selenium nanoparticles. Fig. 4(c) of the SEM revealed that the selenium nanoparticles are uniformly bound to the MCM-41 surface.

FT-Raman spectra

Raman scattering has been proven to be a versatile technique to characterize nanostructured materials. This technique provides information on the crystalline quality of samples and the Raman
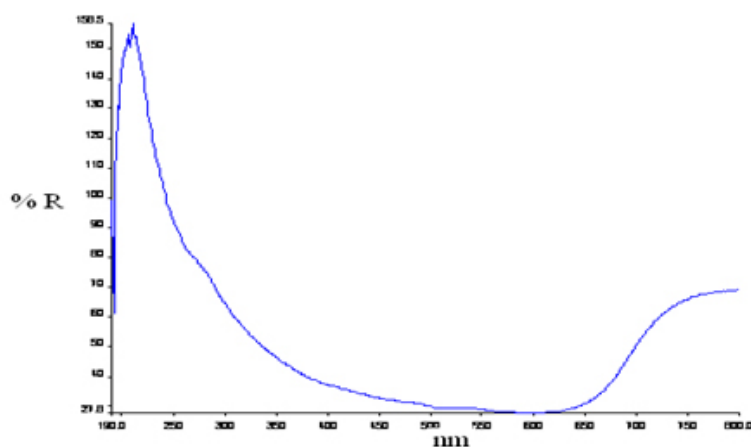

Fig. 6: DR UV-vis spectra of Se-MCM-41

frequency is characteristics for material, structure and the mechanical forces of the crystals which have an effect on the sample[42]. As shown in Fig. 5, an intensive peak at 215 cm^{-1} is observed in the Raman spectra of the Se powder, which is attributed to the Raman scattering of the A_1 mode of hexagonal selenium[26, 42]. The Raman spectrum of as-prepared Se nanoparticles shows a spectral feature similar to that of Se powder. Moreover, pure siliceous MCM-41 characteristic bands at about 918, 542 and 126 cm^{-1} are also observed. They are assigned to Si-OH, six or four-membered ring vibrations and bending mode of Si-O-Si vibrations, respectively[43]. The peak frequency (215 cm^{-1}) of Se nanoparticles indicates that the as-prepared Se nanoparticles have a high degree of crystallinity and the Se nanoparticles are present in the framework of MCM-41. Furthermore, the absence of any signals of the 256 cm^{-1} peak for monoclinic selenium and of the 264-cm^{-1} peak for amorphous selenium indicates that almost no monoclinic selenium or amorphous selenium is present in the prepared samples[26, 44].

UV-visible/ Diffuse reflectance spectroscopy

The UV-vis/DRS spectra of the samples were essential for a proper understanding of the nature of the metal species, especially supporting and complementing previous characterization data of these materials[45]. This is known to be a good technique for the characterization of transition-metal-incorporated zeolites[43]. The UV-vis DRS analysis of Se-MCM-41 was carried out between 200 nm and 800 nm and the representative spectra of the Se-MCM-41 are shown in Fig.6. In Fig. 6, only Se-MCM-41 is shownbecause pure MCM-41 does not have any π and n electrons, hence there is no absorption shown in the spectrum of MCM-41 [46-47].Se-MCM-41shows a band at *ca.* 210 nm which is assigned to selenium in MCM-41 composite[48-50] (which is supported by Raman and XRD). However, in the present study, MCM-41 with amino groups using APTES was modified. Hence, the UV-vis of the sample shows absorption at 210 nm which is attributed to the $\pi \rightarrow \pi^*$ transitions of C=N with selenium[46].

CONCLUSION

In conclusion, we have reported the synthesis of a new composite material. Selenium incorporated to amine functionalized MCM-41 was successfully prepared by impregnation method. The resulting materials were subjected to different characterization techniques, such as XRD, FT-IR, N_2 adsorption-desorption, UV-vis/DRS and Raman – the defining tools which reveal that the Se nanoparticles are firmly attached to the modified MCM-41 support. The XRD pattern shows that the mesoporous nature of the material remains sound after amine and selenium modification. The presence of d (1, 0, 0) in the XRD pattern confirmed the retention of hexagonal ordering even after functionalization and metal complex loading. The effect of selenium loading on the physical properties of MCM-41 (surface area and pore parameters) was explored by nitrogen sorption in which the surface area, pore diameter and pore volume of MCM-41 have decreased with the incorporation of Se into silica framework. UV-Visible spectrometer showed the evidence for the presence of hexagonal Se skeletal structure. The Se–MCM-41 synthesized material may be useful for potential applications in separation and catalysis. This research works on the fabrication and chemistry of mesoporous Se-MCM41 for biomedical applications, and the potential advantages of mesoporous Se-MCM41 in drug delivery.

Many potential applications of mesoporous Se-MCM41 have been explored, from catalysis, separation, biology, environmental monitoring, and pharmaceuticals to clinical toxicology, but a gap in real industrial applications still exists. The great challenge facing the mesoporous material research community now is to transfer laboratory studies to industrial applications. Although the potential applications of such materials have been widely studied in many areas, more efforts are still needed for the continuing study of their practical applications to commercialize mesoporous materials in the future. The forthcoming practical applications in fields such as (metronidazole) drug delivery, biotechnology, gene & protein therapy, new drug delivery system, catalysis, separation, adsorption, electronic devices, low dielectric constant materials and beyond will stimulate more research interests in this area, and more exciting and useful developments in mesoporous materials will also be delivered.

REFERENCES

1. Connor, A. J. O.;Hokura, A.;Kisler, J. M.;Shimazu, S.; Stevens; G. W.; Komatsu, Y. Amino acid adsorption onto mesoporous silica molecular sieves. *Sep Purif Technol.*2006*, 48,* 197-201

2. Liong, M.;Angelos, S.; Choi, E.; Patel, K.;Stoddart, J. F.; Zink, J. I.;Mesostructured multifunctional nanoparticles for imaging and drug delivery.*J Mater Chem.* 2009, *9*, 6251-6257

3. Zhao, S. X.; Lu, Q. G.; Millar, J.G.Advances in mesoporous molecular sieve MCM-41. *IndEngChem Res.*1996,*35,* 2075-2090

4. Scott, B. J.;Wirnsberger, G.;Stucky, G. D. Mesoporous and mesostructured materials for optical applications. *Chem Mater.*2001,*13*, 3140-3150

5. Lim,M. H.;Stein,A. Comparative studies of grafting and direct syntheses of inorganic-organic hybrid mesoporous materials. *ChemMater.*1999*, 11,*3285-3295

6. Zhang, W. H.; Shi, J.L.; Wang, L. Z.; Yan, D. S. Preparation and characterization of ZnO clusters inside mesoporous silica. *Chem. Mater,*2000,*12,* 1408-1413

7. Sayari, A. Catalysisby crystalline mesoporous molecular sieves.*ChemMater.*1996,*8,* 1840-1852

8. Corma, A. From microporous to mesoporous molecular sieve materials and their use in catalysis.*Chem Rev.*1997,*97*, 2373-2420

9. Biz, S., Occelli, M. L. Synthesis and characterization of mesostructured materials. *Catal Rev Sci Eng.*1998,*40*, 329-407

10. Ying, J. Y.;Mehnert, C. P.; Wong M. S. Synthesis and applications of supramolecular-templatedmesoporous materials. *AngewChemInt Ed.*1999,*38*, 56-77

11. Tanev, P. T.;Chibwe, M.;Pinnavaia, T. J. Titanium-containing mesoporous molecular sieves for catalytic oxidation of aromatic compounds. *Nature.*1994; *368:* 321-323

12. Corma, A.; Navarro, M. T. ; Pariente, J. P. Synthesis of an ultralarge pore titanium silicate isomorphous to MCM-41 and its application as a catalyst for selective oxidation of hydrocarbons.
    *J Chem Soc ChemCommun.*1994,*2*, 147-148

13. Yuan ZY, Liu SQ, Chen TH, Wang JZ, Li HX. Synthesis of iron-containing MCM-41.
    *J ChemSocChemCommun.*1995; *9*: 973-974.

14. Reddy, K. M.;Moudrakovski, I.;Sayari, A. Synthesis of mesoporous vanadium silicate molecular sieves.*J ChemSocChemCommun.*1994,*9,* 1059-1060

15. Zendehdel, M.;Cruciani, G.;Kar, F.;Barati, A. Synthesis and study the controlled release of metronidazole from the new PEG/NaY and PEG/MCM-41 nanocomposites. *J Environ Health Sci Eng.*2014,*12*, 35-39

16. Gao, B.; Fang, L.; Men, J.; Zhang, Y. Preparation of grafted microspheres CPVA-g-PSSS and studies on their drug-carrying and colon-specific drug delivery properties. *Mater SciEng C.* 2013,*33,*1300–1306

17. Popova, M. D.;Szegedi, A.;Kolev, I. N.; Mihály, J.;Tzankov, B. S.;Momekov, G. T. Carboxylic modified spherical mesoporoussilicasàs drug delivery carriers. *Int J Pharm.*2012,*436*, 778–785

18. Liu, M. Z.; Zhang, S. Y.;Shen, Y. H.; Zhang, M. L. Selenium nanoparticles prepared from reverse microemulsion process.*Chinese ChemLett.*2004*, 15,* 1249-1252

19. Shin, Y.; Blackwood, J. M.;Bae, I.;Arey,

B.W.Exarhos GJ. Synthesis and stabilization of selenium nanoparticles on cellulose nanocrystal.*Mater.Lett.*2007*, 61,*4297-4300

20. Zhang, S.; Zhang, J.; Wang, H.; Chen, H. Synthesis of selenium nanoparticles in the presence of polysaccharides. *Mater Lett,*2004*, 58*, 2590-2594

21. Prosser, V. The optical constants of single crystals of hexagonal selenium.*Czech. J. Phys. B*. 1960,*10*, 306

22. Li, Y. ; Yan, B. Lanthanide (Tb^{3+}, Eu^{3+}) functionalized MCM-41 through modified *meta*-aminobenzoic acid linkage: covalently bonding assembly, physical characterization and photoluminescence. *MicroporMesoporMater.*2010,*128*, 62-70

23. Pires, L. H. ;Queiroz, R. M. ;Souza, R. P. ; da Costa, C. E. F. ;Zamian, J. R. ; Weber, I. T. Synthesis and characterization of spherical Tb-MCM-41.*J Alloys Compo.*2010,*490*, 667-671

24. Shekar, N. V. C.;Rajan, K. G.;Rajagopalan, S.;Yousuf, M. Growth of hexagonal selenium crystals: observation of new growth morphologies. *Bull Mater Sci.*1993,*16*, 171-175

25. Lei, Y.; Yao, L.; He, Y.; Wang, S.; Yu, R.;Zou, B. Preparation of single-crystalline selenium nanowires in the presence of ethylenediaminetetramethylenephosphonic acid. *ChemLett.* 2006,*35*, 330-331

26. Lei, R.;Hongzhou, Z.;Pingheng, T.;Yaofeng, C.;Zhensheng, Z.;Yongqin, C. Hexagonal selenium nanowires synthesized via vapor-phase growth. *J PhysChem B.*2004,*108*, 4627-4630

27. Puanngam, M.;Unob, F. Preparation and use of chemically modified MCM-41 and silica gel as selective adsorbents for Hg(II) ions. *J Hazard Mater.*2008,*154*, 578-587

28. Zheng, Y.; Li, Z.;Zheng, Y.;Shen, X.; Lin, L. Synthesis and characterization of Fe–Ce–MCM-41.*Mater Lett.*2006,*60*, 3221-3223

29. Yang, X.;Zhou, L.;Chen, C.;Li, X.;Xu, J. Direct synthesis and characterization of bifunctional Me–Zr-MCM-41.*Mater Lett.*2009,*63,* 1754-1756

30. Giorgi, R.;Bozzi, C.; Dei, L.;Gabbiani, C.;Ninham, B. W.;Baglioni, P. Nanoparticles of Mg(OH)$_2$: Synthesis and application to paper conservation. *Langmuir.*2005,*21*,8495-8501

31. Hall, B. D.;Zanchet, D.;Ugarte, D. Estimating nanoparticle size from diffraction measurements. *J.ApplCryst.* 2000*, 33,* 1335-1341

32. Zhang, X. ; Zhang, C. ; Guo, H. ; Huang, W. ;Polenova, T. ;Francesconi, L. C. Optical spectra of a novel polyoxometalate occluded within modified MCM-41.*J PhysChem B.*2005,*109,*19156-19160

33. Borrego, T.; Andrade, M.; Pinto M. L.; Silva, A. R.;Carvalho, A. P.; Rocha, J. Physicochemical characterization of silylated functionalized materials. *J Colloid Interf Sci.* 2010,*344*, 603-610

34. Parida, K. M.;Rath, D. Amine functionalized MCM-41: An active and reusable catalyst for Knoevenagel condensation reaction. *J MolCatal A: Chemical.*2009,*310*, 93-100

35. Parida, K. M.;Rath, D.; Dash, S. S. Synthesis, characterization and catalytic activity of copper incorporated and immobilized mesoporous MCM-41 in the single step amination of benzene.
*J MolCatalA:Chemical.*2010,*318,* 85-93

36. Espinosa, M. ; Pacheco, S. ; Rodriguez, R. Synthesis and characterization of NH$_2$-porphyrins covalently immobilized on modified-SBA-15.*J Non-CrystallineSolids.*2007,*353*, 2573-2581

37. Selvaraj, M.;Sinha, P. K.; Lee, K.;Ahn, I.;Pandurangan, A.; Lee, T. G. Synthesis and characterization of Mn-MCM-41and Zr-Mn-MCM-41. *Micr.Meso.Mater.*2005,*78*, 139-149

38. Cai, Q.;Luo, Z.; Pang, W.; Fan, Y.; Chen, X.; Cui, F. Dilute solution routes to various controllable morphologies of MCM-41 silica with a basic medium. *Chem Mater.2001, 13*, 258-263

39. Chao, K. J. ; Wu, C. N. ; Chang, A. S. ; Hu, S. F. The study of MCM-41 molecular sieves by energy-filtering TEM. *MicroporMesopor Mater.*1999*, 27,* 287-295

40. Kruk, M.;Jaroniec, M.; Sakamoto, Y.;Terasaki, O.;Ryoo, R.;Ko, C. H. Determination of pore size and pore wall structure of MCM-41 by using nitrogen adsorption, transmission electron microscopy, and X-ray diffraction. *J PhysChemB.*2000,*104*, 292-301

41.   Caponetti, E. ;Minoja, A. ;Saladino, M. L. ;Spinella, A. Characterization of Nd–MCM-41 obtained by impregnation.*MicroporMesopor Mater.*2008, *113*, 490-498

42.   Lewis, L. R.; Edwards, H. G. Handbook of Raman Spectroscopy, CRC Press New York, 2001

43.   Rana, R. K.;Viswanathan, B. Mo incorporation in MCM-41 type zeolite. *Catalysis Letters.*1998,*52*, 25-29

44.   Jagminas, A.;Gailiûtë, I.;Niaura, G.;Giraitis, R. Template-assisted fabrication of pure Se nanocrystals in controllable dimensions. *Chemija.*2005,*16,* 15-20

45.   Soundiressane, T.;Selvakumar, S.;Menage, S.; Hamelin, O.;Fontecave, M.; Singh, A. P.Ru- and Fe-based *N,N*2-bis(2-pyridylmethyl)- *N*-methyl-(1*S*,2*S*)-1,2-cyclohexanediamine complexes immobilised on mesoporous MCM-41: Synthesis, characterization and catalytic applications. *J MolCatal A- Chem.* 2007,*270,* 132-143

46.   Zhao, D.; Zhao, J.; Zhao, S.; S.; He, L.; Wang, W. Preparation of MCM-41-supported chiral SalenMn (III) catalysts and their catalytic properties in the asymmetric epoxidation of olefins.*Chinese Sci. Bull.*2007*, 52,*2337- 2344

47.   EsmatIzadpanah and Sayyahi, S.Fe- Containing Ionic Liquid Supported on Nanosized MCM-41: An Efficient and Reusable Catalyst in the Synthesis of 2-Aryl Benzimidazole Derivatives. *Oriental Journal of Chemistry.*2016, *32*(5), 2101-2106

48.   Prosser, V.;Henisch, H. K. Diffuse reflectivity of selenium. *Mat. Res. Bull.*1967,*2*, 75-83

49.   Jacob, C.;Maret, W.;Vallee, B. L. Selenium redox biochemistry of zinc–sulfur coordination sites in proteins and enzymes. *Proc. Natl. Acad. Sci.*1999,*96*, 1910-1914

50.   Goldbach, A.;Saboungi, M.L. Optical spectroscopy on Se clusters and chains confined in zeolites.*Eur. Phys. J. E.*2003,*12*,185-190